Simple and double modulations in $Bi_{2-x}Pb_xSr_2CaCu_2O_{8+\delta}$

N. Jakubowicz, D. Grebille, M. Hervieu, and H. Leligny
Laboratoire CRISMAT (UMR CNRS 6508), ISMRA, Boulevard du Maréchal Juin, 14050 Caen Cedex, France
(Received 15 June 2000; published 9 May 2001)

Two single crystals of the Pb-doped high-T_c superconductor $Bi_{2-x}Pb_xSr_2CaCu_2O_{8+\delta}$ phase have been isolated with $x=0.4$ and 0.2. In the first case, the structure is monoincommensurately modulated with the so-called Pb-type modulation ($\mathbf{q_{II}}=0.11\mathbf{b}^\star$). In the second case, the structure is characterized by a double modulation ($\mathbf{q_I}=0.2\mathbf{b}^\star+\mathbf{c}^\star$; $\mathbf{q_{II}}=0.15\mathbf{b}^\star$). The two modulated structures have been refined from single-crystal x-ray diffraction data using the four- and five-dimensional superspace groups' formalism, respectively. Considering these substituted phases and the well-known lead-free phase, the same symmetry is observed for their average structures, while their structural modulations exhibit significant discrepancies. Different disordered regions are characterized in relation to the modulation period. The results are confirmed by high-resolution electron-microscopy observations. The relative structures are compared with each other and the structure of the lead-free phase, particularly about the stacking scheme of the structural layers.

DOI: 10.1103/PhysRevB.63.214511 PACS number(s): 74.72.Hs, 61.44.Fw, 61.10.−i, 61.66.Fn

I. INTRODUCTION

Bi-based high-T_c superconductor oxides have been widely investigated over the last twelve years for their interesting structural and physical properties. Especially in the (Bi,Pb)SrCaCuO system, several structural models have been proposed for the lead-free $Bi_2Sr_2CaCu_2O_{8+\delta}$ phase,[1–6] in order to describe in a proper way complex modulation phenomena. The corresponding very large modulated displacements can be only roughly approximated in a supercell model, and so need an appropriate description in the superspace formalism for aperiodic structures. It is now well established that there is no direct correlation between superconductivity and incommensurability in these compounds. Nevertheless, it appears that small variations of stoichiometry can induce slight structural modifications and simultaneously significant changes of the physical properties, and so it is important to give a better insight into this complex structure as a function of oxygen content or cationic substitutions.

It is also well known by different characterizations that this structure involves different kinds of structural defects, which can be in close relation with the displacive or substitutional modulation waves and can also have an effect upon physical properties. One of the signatures for such structural defects lies in the observation made on the diffraction patterns of diffuse scattering between usual satellite reflections predicted by the structural model ($\mathbf{q_I}=0.21\mathbf{b}^\star+\mathbf{c}^\star$) [Fig. 1(a)], lying now at forbidden nodes of the four-dimensional reciprocal lattice. Different hypotheses have been given to explain their origin, and two main and contradictory conclusions have been proposed.

First, they can be related to the crystal quality and preparation only. Arguments for this explanation maintain that these diffuse intensities depend on the observed samples and their mosaic spread.[7,8] Nevertheless, their systematic observation, even in high-quality samples, outlines their intrinsic character.[9–11] Moreover, a lot of studies have shown that these unexplained diffusions clearly depend on the substitution of Bi for Pb.[12–15] They become sharper and one observes an important increase in the modulation period. They become independent satellite reflections for a second type of modulation that has been called the Pb-type modulation superimposed to the classical Bi one. This leads to the second explanation for these diffused intensities: they are related to a new type of modulated structure. This Pb-type modulation is then characterized by a new modulation vector $\mathbf{q_{II}}=0.12\mathbf{b}^\star$ without any rational component along $\mathbf{c}^\star$ [Fig. 1(b)]. With increasing Pb rate, electron-microscopy studies have shown that the first modulation disappears, with diffuse or absent Bi-type satellite reflections, and the structure can then be described only by this new type of modulation [Fig. 1(c)]. No structure refinement of this new modulation has been proposed for the moment, but hypotheses can be proposed taking into account a new stacking scheme of the structural cationic slabs[16,17] or relative shifts of the slabs with respect to each other, as evidenced by TEM observations.[13,18] These explanations are also related to some descriptions of the 2212 phase using a monoclinic symmetry, probably resulting from this type of mutual layer shift.[19,6]

In the intermediate range where the two types of satellite reflections are simultaneously observed, a question arises regarding the independence of both modulations. Indeed, one can easily imagine the existence of independent modulated domains. But this last hypothesis was discarded because the observation of additional intermodulation satellite reflections[15,20,21] proved the existence of a doubly modulated

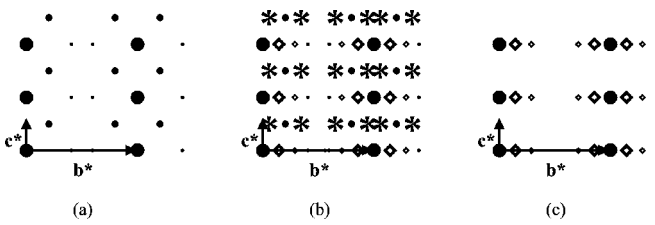

FIG. 1. Schematic representation of diffraction pattern corresponding to (a) modulation *I* (dark circles; first- and second-order satellite reflections), (b) double modulation (stars represent intermodulation satellites), and (c) modulation *II* (open diamonds; first- and second-order satellite reflections).

state. However only qualitative interpretations of these reflections could be given and the modulated structure has not been refined.

Such a double-modulation state has also been observed in the case of the 2201-type structure and a structural refinement has been proposed in this case,[22] leading to relatively poor agreement factors. One of the conclusions of this study was the ''in-phase stacking'' of the successive layers, corroborating the model proposed by Tolédano *et al.*,[17] but some interatomic distances or modulated displacements can be considered as doubtful in this study.

In the present study, a single crystal of the highly Pb-doped phase has been synthesized and characterized by the specific diffraction pattern of the Pb-type modulation (modulation vector $\mathbf{q_{II}}=0.11\mathbf{b}^\star$ without any rational component along $\mathbf{c}^\star$). The structure refinement of this phase from x-ray-diffraction data allows us to describe this modulation alone and to compare it with the usual Bi-type modulation. Then, starting with the knowledge of these two independent modulations, it was possible to initiate in a proper way the modulated displacements characteristic of the double-modulated 2212 phase, using another single-crystal x-ray-diffraction data set. A new structure refinement was then possible, using the five-dimensional (5D) superspace formalism to take into account specifically the different classes of satellite reflections.

II. EXPERIMENTAL PROCEDURE

Single crystals of $Bi_{2-x}Pb_xSr_2CaCu_2O_{8+\delta}$ ($x=0.2$ and 0.4) were prepared by the self-flux method from a mixture of Bi_2O_3, $SrCO_3$, $CaCO_3$, CuO, and PbO in the proportion Bi:1.4:Pb:0.6:Sr:2:Ca:1:Cu:2 for crystal *A* and Bi:1.7:Pb:0.36:Sr:1.3:Ca:1.3:Cu:2 for crystal *B*. The precursor materials were first decarbonated at 800 °C for 12 h. The resulting powders were then heated at 1010 °C for crystal *A* and at 1040 °C for crystal *B* in an aluminum crucible, then cooled down to room temperature.

A platelet single crystal could be extracted from each preparation. Crystal quality was tested using a Weissenberg camera. A first estimation of crystal parameters and symmetry was then obtained.

Crystal A ($0.24\times0.22\times0.012$ mm^3) showed a diffraction pattern with satellite reflections in position $0.11\mathbf{b}^\star$ [Fig. 1(c)], corresponding to the modulation *II* (also called Pb-type modulation). Weak diffuse scattering in position $\mathbf{q_I}$, corresponding to modulation *I*, was observed. The presence of some additional disorder was determined from the observation of diffused streaks. Energy dispersive spectroscopy (EDS) analyses confirmed the presence of lead in a constant ratio for Pb/Cu of 0.2. No trace of Al due to a contamination by the crucible could be detected, in the limit of accuracy of the analysis technique. The cationic compositions varied between two extreme limits, namely, $Bi_{1.9}Pb_{0.4}Sr_{1.85}Ca_{0.8}Cu_2$ and $Bi_{1.6}Pb_{0.4}Sr_2Ca_{0.9}Cu_2$, according to the samples. These analyses showed that there was a significant calcium deficiency with regard to the ideal composition 2212 as well as a possible Sr/Bi balance. Note that no straightforward variation of the *q* value had been correlated to the cation contents.

Crystal B ($0.3\times0.06\times0.014$ mm^3) presented a diffraction pattern characterized by three sets of satellite reflections, respectively, in position $\mathbf{q_I^\star}$, $\mathbf{q_{II}}$, and $\mathbf{q_I}\pm\mathbf{q_{II}}$ [Fig. 1(b)]. A least-square refinement on θ values of 20 reflections lead to $\mathbf{q_I}=0.200(3)\mathbf{b}^\star+\mathbf{c}^\star$ and $\mathbf{q_{II}}=0.150(2)\mathbf{b}^\star$ for modulation *I* and *II*, respectively. Additional reflections compared with the usual diffraction pattern outlined the presence of 90° twin domains in the crystal, according to the pseudotetragonal character of the cell. EDS analyses had been performed on this preparation and gave the cationic composition $Bi_2Pb_{0.25}Sr_{1.74}CaCu_2$. No trace of Al was detected.

For both crystals, the intensities of the main and satellite reflections up to second order were measured at room temperature using a CAD4 Enraf-Nonius diffractometer. The absence of any rational component and the small irrational value of the $\mathbf{q_{II}}$ modulation vector implied that main and satellite reflections were very close in reciprocal space (Fig. 1). As a consequence, it was not possible to separate the corresponding contributions using Mo Kα radiation. The two collections were then measured using Cu Kα radiation (1.5418 Å).

For the double modulation (crystal *B*) three data sets were independently recorded: (i) main reflections, (ii) satellite reflections for modulation *I* ($\pm\mathbf{q_I}$, $\pm2\mathbf{q_I}$), and (iii) second-order satellites of modulation *I* ($\pm2\mathbf{q_I}$) and intermodulation satellite reflections ($\mathbf{q_I}\pm\mathbf{q_{II}}$). Experimental data for both crystals are summarized in Table I.

Electron-diffraction study was carried out with a JEOL 200CX electron microscope working at 200 kV. High-resolution images were taken with the microscope TOPCON 002B that had a resolution of 0.18 nm.

III. STRUCTURAL REFINEMENTS

According to the incommensurate character of the structures, the superspace formalism for modulated structures was used.[23] The atomic modulated displacements u^i are expressed by their Fourier expansion as a function of the internal parameters $\overline{x_4}=\mathbf{q_I}\cdot\mathbf{r}$ and $\overline{x_5}=\mathbf{q_{II}}\cdot\mathbf{r}$, as

$$u^i(\overline{x_4},\overline{x_5})=\sum_{p,q}A^i_{p,q}\sin 2\pi(p\overline{x_4}+q\overline{x_5}) + \sum_{p,q}B^i_{p,q}\cos 2\pi(p\overline{x_4}+q\overline{x_5}),\quad i=1-3, \tag{1}$$

where $\mathbf{r}$ is the average atomic position in a given unit cell and *p* and *q* are integers.

In the same way, the site-occupation and the thermal atomic displacement parameters can be modulated, respectively, as

$$P(\overline{x_4},\overline{x_5})=\sum_{p,q}[C_{p,q}\sin 2\pi(p\overline{x_4}+q\overline{x_5}) + D_{p,q}\cos 2\pi(p\overline{x_4}+q\overline{x_5})], \tag{2}$$

TABLE I. Experimental data.

	Crystal *A*	Crystal *B*
Chemical formula	$Bi_{1.69}Pb_{0.4}Sr_{2.0}Ca_{0.88}Cu_{2.05}O_{8.03}$	$Bi_{1.8}Pb_{0.2}Sr_{2.0}Ca_{0.9}Cu_{2.0}O_{8.1}$
Crystal size (mm^3)	$0.240\times0.22\times0.012$	$0.300\times0.060\times0.014$
Cell parameters (Å)	$a=5.4031(7)$ $b=5.3759(5)$ $c=30.779(5)$	$a=5.395(1)$ $b=5.405(1)$ $c=30.772(5)$
T(K)	294	
Modulation vector	[0,0.110(1),0]	[0,0.200(3),1] [0,0.150(2),0]
Superspace group	$Bbmb(0\beta0)00s$	$Bbmb(0\beta1,0\gamma0)000,00s$
Z	4	
Data collection	CAD4 Enraf-Nonius diffractometer	
Wavelength (Å)	λ (CuK α) = 1.5418	
Absorption coefficient (cm^{-1})	1014	
Registered space	h:0,6;k:−6,6;l:0,38;m:−2,2	h:0,6;k:0,6;l:0,38;m:−2,2;n:−1,1
Number of measured reflections	10170	7284
Number of reflections with $I>3\sigma(I)$	1193	1752
Number of refinement parameters	107	126
$R,wR(hklm)$	0.062, 0.070	0.063, 0.061
$R,wR(hkl0)$	0.069, 0.071	0.044, 0.044
N_0	400	404
$R,wR(hkl1)$	0.052, 0.061	0.062, 0.066
N_1	602	911
$R,wR(hkl2)$	0.095, 0.132	0.132, 0.151
N_2	191	437

$$U^{ij}(\overline{x_4},\overline{x_5})=\sum_{p,q}\left[u^{ij}_{p,q}\sin 2\pi(p\overline{x_4}+q\overline{x_5})+v^{ij}_{p,q}\cos 2\pi(p\overline{x_4}+q\overline{x_5})\right]. \quad (3)$$

Structural refinements were performed using the JANA98 package for modulated structures.[24] Modulated displacements were initiated from the known values for the pure phase.[5]

A. The Pb-type monoincommensurate structure (crystal *A*)

The modulated structure of this crystal was refined in the four-dimensional superspace formalism using the $\overline{x_5}$ internal parameter. The observed reflection conditions ($hklm:h+l=2n$, $0klm:k=2n$, and $hk0m:k+m=2n$) are compatible with the superspace group $Bbmb(0\beta0)00s$ (Table II). This group differs from the corresponding one $Bbmb(0\beta1)$ observed for the nondoped compound, first by the absence of any rational component for the modulation vector and second by the internal translation associated with the glide mirror *b*, orthogonal to the **c** direction. Actually, when considering the symmetry constraints for the atoms in special positions in the structure, these two new features are correlated in order to allow similar modulated displacements as in the Pb-free 2212 phase.

In the previous refinement of the undoped 2212 cuprate phase, it was necessary to introduce a split-atom model for Bi outside the mirror plane perpendicular to *y* and an occupation modulation of the corresponding sites. Such a splitting

TABLE II. Symmetry operations for superspace groups Bbmb($0\beta1$) (lead-free phase), Bbmb($0\beta0$)0ss (crystal *A*), and Bbmb($0\beta1,0\gamma0$)000,00*s* (crystal *B*).

$Bbmb(0\beta1)$	$Bbmb(0\beta0)00s$	$Bbmb(0\beta1,0\gamma0)000,00s$
$(\frac{1}{2},0,\frac{1}{2},\frac{1}{2})+$	$(\frac{1}{2},0,\frac{1}{2},0)+$	$(\frac{1}{2},0,\frac{1}{2},\frac{1}{2},0)+$
x,y,z,x_4	x,y,z,x_5	x,y,z,x_4,x_5
$-x,y+\frac{1}{2},z,x_4$	$-x,y+\frac{1}{2},z,x_5$	$-x,y+\frac{1}{2},z,x_4,x_5$
$x,-y,z,-x_4$	$x,-y,z,-x_5+\frac{1}{2}$	$x,-y,z,-x_4,-x_5+\frac{1}{2}$
$-x,-y+\frac{1}{2},z,-x_4$	$-x,-y+\frac{1}{2},z,-x_5+\frac{1}{2}$	$-x,-y+\frac{1}{2},z,-x_4,-x_5+\frac{1}{2}$
+ Inversion centre	+ Inversion centre	+ Inversion centre

TABLE III. Refinement results for crystal *A*: positions (A_i, B_i) and occupations (A_i', B_i'). $0^\star$ were fixed during refinement because they were not significant. $0^\dagger$ are constrained by symmetry.

		$A_0(P_0)$	$A_1(C_1)$	$B_1(D_1)$	$A_2(C_2)$	$B_2(D_2)$
Bi	u_1	0.2287(1)	$0^\star$	$0^\star$	0.0007(2)	0.0023(2)
	u_2	0.5225(2)	-0.0183(3)	0.0372(6)	-0.0141(2)	-0.0039(5)
	u_3	0.05137(4)	0.00860(3)	0.00242(6)	0.00282(4)	0.00099(4)
	P	0.511(1)	-0.327(9)	$0^\star$	$0^\star$	$0^\star$
Sr	u_1	0.2528(2)	$0^\star$	$0^\star$	$0^\star$	$0^\star$
	u_2	0.007(1)	-0.007(9)	0.023(1)	-0.0033(6)	-0.011(1)
	u_3	0.13901(3)	0.00871(7)	$0^\star$	-0.0009(2)	0.00032(5)
	P	0.488(2)	$0^\star$	0.21(1)	$0^\star$	$0^\star$
Ca	u_1	0.25	$0^\star$	$0^\dagger$	$0^\dagger$	$0^\dagger$
	u_2	$0^\dagger$	$0^\dagger$	$0^\dagger$	$0^\star$	$0^\dagger$
	u_3	0.25	0.0093(1)	$0^\dagger$	$0^\dagger$	$0^\dagger$
	P	0.864(2)	$0^\dagger$	$0^\dagger$	$0^\dagger$	-0.026(4)
Cu	u_1	0.2506(3)	$0^\star$	$0^\dagger$	$0^\dagger$	$0^\star$
	u_2	0.5	$0^\dagger$	0.0087(2)	-0.0020(4)	$0^\dagger$
	u_3	0.19597(4)	0.00869(7)	$0^\dagger$	$0^\dagger$	0.00029(8)
OC1	u_1	$0^\dagger$	$0^\dagger$	$0^\dagger$		
	u_2	0.25	$0^\dagger$	0.010(2)		
	u_3	0.1975(2)	0.0095(4)	$0^\dagger$		
OC2	u_1	0.5	$0^\dagger$	$0^\star$		
	u_2	0.25	$0^\dagger$	0.010(2)		
	u_3	0.1989(2)	0.0089(4)	$0^\dagger$		
OS	u_1	0.299(3)	-0.025(2)	0.035(6)		
	u_2	0.452(4)	0.026(2)	-0.005(5)		
	u_3	0.1163(2)	0.0068(3)	$0^\star$		
	P	0.52(1)	0.05(1)	-0.43(3)		
OB	u_1	0.138(4)	0.004(3)	0.022(5)		
	u_2	0.113(4)	-0.038(3)	$0^\star$		
	u_3	0.0547(3)	0.0104(5)	$0^\star$		
	P	0.44(1)	0.11(2)	0.38(1)		

for Bi is also involved in crystal *A*. Moreover, it appeared that such a splitting was also necessary for Sr and for the oxygen atoms OB and OS of the [BiO] and [SrO] layers, respectively. The corresponding sites are symmetry related and are characterized by complementary occupation functions, so that according to the internal phase of the modulation, these different sites can be alternately occupied. This point will be discussed further.

Anisotropic thermal motion parameters were taken for cations and isotropic ones for oxygen atoms. A modulation of these terms was also introduced for Bi, Sr, and Cu atoms. A substitution of Bi for Ca was also introduced and lead to a substitution rate of 14%. This result is compatible with the measured composition. In the lead-free cuprate phase, the same type of substitution was observed with a weaker refined rate of approximately 7.8%. The final agreement factors were $R=0.062$, $R_0=0.069$, $R_1=0.052$, and $R_2=0.095$ for main reflections and first- and second-order satellites, respectively. Refinement results are reported in Tables III and IV.

B. The double-modulated structure (crystal *B*)

The average structure is still characterized by the same symmetry space group $Bbmb$. The respective reflection conditions previously observed for the two independent monoincommensurate structures are still observed, resulting now in a five-dimensional centering of the cell (0.5, 0, 0.5, 0.5, 0) and in the five-dimensional superspace group $Bbmb(0\beta1,0\gamma0)0,00s$ (Table II). Note that the four-dimensional superspace groups of the independent monoincommensurate structures are subgroups of the 5D superspace group of the double-modulated structure.

Results concerning the first modulation are well known. Structural refinement of the second structural modulation has been performed with crystal *A*. All these results have been used for initiating positional and occupational Fourier terms in the present 5D study, neglecting in a first step coupled terms involving both modulations simultaneously. Then, these coupled terms were refined in order to take into account the measured intensities of intermodulation reflections with $m=\pm1$ and $n=\pm1$ simultaneously.

According to the observed Fourier maps and to the previous structural results, a similar split-atom model was introduced for Bi and OB atoms in the [BiO] layers characterized by a harmonic occupation modulation. One could expect the presence of vacancies for the oxygen sites OS of the [SrO] layers, but the limitations of the JANA98 software in the 5D

TABLE IV. Thermal displacement parameters for crystal $A(Å^2)$. $0^\star$ were fixed during refinement because they were not significant. $0^\dagger$ are constrained by symmetry.

		U_0	sin1	cos1
Bi	U_{eq}	0.0172(1)		
	U_{11}	0.0229(3)	-0.0036(3)	-0.006(1)
	U_{22}	0.0182(3)	$0^\star$	-0.0093(6)
	U_{33}	0.0104(2)	-0.0040(2)	-0.0053(5)
	U_{12}	$0^\star$	0.0031(7)	$0^\star$
	U_{13}	-0.0005(2)	$0^\star$	-0.0020(7)
	U_{23}	$0^\star$	-0.0027(3)	-0.0013(1)
Sr	U_{eq}	0.0195(4)		
	U_{11}	0.0136(6)	-0.0015(6)	$0^\star$
	U_{22}	0.022(1)	-0.0154(7)	-0.010(2)
	U_{33}	0.0232(6)	-0.0027(7)	-0.009(2)
	U_{12}	0.003(2)	$0^\star$	-0.002(1)
	U_{13}	0.0034(6)	$0^\star$	-0.006(2)
	U_{23}	-0.008(1)	$0^\star$	0.007(1)
Ca	U_{eq}	0.0168(5)		
	U_{11}	0.011(1)		
	U_{22}	0.0141(9)		
	U_{33}	0.0249(7)		
	U_{12}	$0^\dagger$		
	U_{13}	$0^\star$		
	U_{23}	$0^\dagger$		
Cu	U_{eq}	0.0139(4)		
	U_{11}	0.0111(9)	$0^\star$	$0^\dagger$
	U_{22}	0.0071(7)	-0.0031(7)	$0^\dagger$
	U_{33}	0.0235(6)	-0.002(1)	$0^\dagger$
	U_{12}	$0^\dagger$	$0^\dagger$	$0^\star$
	U_{13}	$0^\star$	0.0023(9)	$0^\dagger$
	U_{23}	$0^\dagger$	$0^\dagger$	0.0041(5)
OC1	U_{iso}	0.023(1)		
OC2	U_{iso}	0.024(1)		
OS	U_{iso}	0.032(2)		
OB	U_{iso}	0.029(2)		

formalism did not allow us to use crenel functions that would have been adequate to describe such vacancies. As a consequence, this site was considered as fully occupied in the whole internal space.

A substitution of Bi for Ca was also considered as in the previous structure and lead to a substitution rate of 10%, which is an intermediate value between the previously reported values for the first (7%) and the second (14%) modulations.

Anisotropic thermal atomic displacement parameters have been taken for cations and isotropic ones for oxygen atoms. A modulation of these terms has also been introduced for the Bi atom. The twin volume ratio has also been refined to a final value of 7.7%. The global agreement factor for this double modulation is $R=0.063$ with 0.044 for main reflections, 0.062 for first-order satellites, and 0.132 for second-order satellites of modulation *I* and for intermodulation satellites.

One can notice here that the agreement concerning the intermodulation satellite reflections with $m=\pm 1$ and $n=\pm 1$ is quite satisfactory and directly depends on intermodulation terms involving $x_4 \pm x_5$ in the Fourier expansion of the modulation functions. The refinement results are given in Tables V–VII.

IV. DISCUSSION

A. The monoincommensurate modulated structure of $Bi_{1.6}Pb_{0.4}Sr_2Ca_{0.9}Cu_2O_8$

The structure of crystal *A* is closely related to the well-known 2212 modulated structure.[5] The average structure is the same with the same stacking along the **c** direction of BiO-SrO-CuO_2-Ca-CuO_2-SrO-BiO slabs. But the absence of any rational component $\mathbf{c}^\star$ for the modulation vector implies that the relative modulation functions concerning two consecutive slabs separated by **c**/2 are in phase, whereas they were out of phase for the previous structure. As a consequence, the slabs were present in phase corrugations (Fig. 2). We have already outlined that this point is also related to the difference in the superspace symmetry group involving an internal phase translation of one-half associated with the glide mirror plane **b** orthogonal to **c**, allowing modulated atomic displacements along the **c** direction. It is also the reason for the unexplained absence of first-order type-*II* satellite reflections observed around the (040) reflection in Fig. 6 of J. Zhu *et al.*[11]

It is interesting to compare the displacement modulation functions along **b** and **c** for both structures. These functions are drawn in Figs. 3 and 4 (for a comparison with the previous study of the lead-free phase,[5] a phase shift of 0.25 was applied). Within the two types of crystals, the displacement amplitudes along *z* are quite similar while along *y*, a half amplitude is observed for crystal *A*. This last feature can be easily understood: for equivalent displacements along *z*, a double-modulation period ($\mathbf{q_I}=0.12$ versus $\mathbf{q_I}=0.21$) results in a half curvature of the slabs, and, as a consequence, in half-*y* longitudinal modulated displacements.

These results are confirmed by high-resolution electron microscopy. An enlargement of a typical [001] HREM image is given in Fig. 5. It can be compared to the corresponding HREM image of the lead-free 2212 cuprates, which have been extensively reported. In this last case, the contrast generated by the modulation appears as straight rows of darker or brighter dots (depending on the focus value). In the present phase, one observes that the average direction of modulation is actually **b** but the rows of bright and dark dots are blurred and not strictly straight. The wavy patterns in the [100] images confirm the 2212 stacking mode of the layers (Fig. 6) (see also Fig. 3 in Ref. 20) and a double periodicity of the modulation along **b**. Two rows of dots marked with black arrows are attributed to the [(Bi,Pb)O] layers. The double [BiO] layers undulate in phase along **c** (behavior expected for an orthorhombic modulated supercell) but a detailed analysis shows that the phenomenon is more complex. For example, equivalent zones of the waves are indicated by triangles in Fig. 6. The white triangles (upper part of the image) are aligned along **c**, in an area that is

TABLE V. Refinement results for crystal *B*: positions (A_{ij},B_{ij}) and occupations (P). $0^{\star}$ were fixed during refinement because they were not significant. $0^{\dagger}$ were constrained by symmetry.

		$A_0(P_0)$	$A_{1,0}(A'_{1,0})$	$B_{1,0}(B'_{1,0})$	$A_{0,1}(A'_{0,1})$	$B_{0,1}(B'_{0,1})$
Bi	u_1	0.2267(1)	$0^{\star}$	-0.00450(9)	$0^{\star}$	$0^{\star}$
	u_2	0.5169(5)	0.0302(8)	-0.0049(4)	-0.04420(7)	0.02698(9)
	u_3	0.051492(9)	$0^{\star}$	0.00350(1)	0.00607(2)	0.01061(1)
	P	0.5131(9)	0.564(2)	$0^{\star}$	$0^{\star}$	0.046(2)
Sr	u_1	0.25259(9)	$0^{\dagger}$	$0^{\star}$	$0^{\star}$	$0^{\dagger}$
	u_2	0	0.0415(1)	$0^{\dagger}$	$0^{\dagger}$	0.0241(3)
	u_3	0.14017(1)	$0^{\dagger}$	-0.00685(3)	0.00663(3)	$0^{\dagger}$
Ca	u_1	0.25	$0^{\star}$	$0^{\star}$	0.0010(6)	$0^{\dagger}$
	u_2	$0^{\dagger}$	$0^{\dagger}$	$0^{\dagger}$	$0^{\star}$	$0^{\dagger}$
	u_3	0.25	$0^{\dagger}$	-0.00782(8)	0.00616(9)	$0^{\dagger}$
	P	0.894(1)	$0^{\dagger}$	$0^{\dagger}$	$0^{\dagger}$	$0^{\dagger}$
Cu	u_1	0.2498(1)	$0^{\dagger}$	$0^{\dagger}$	$0^{\dagger}$	$0^{\star}$
	u_2	0.5	0.0118(2)	$0^{\star}$	$0^{\star}$	0.0073(4)
	u_3	0.19657(3)	$0^{\star}$	-0.00862(4)	0.00715(5)	$0^{\star}$
OC1	u_1	$0^{\dagger}$	$0^{\dagger}$	$0^{\star}$	$0^{\star}$	$0^{\dagger}$
	u_2	0.25	0.013(1)	$0^{\dagger}$	$0^{\dagger}$	$0^{\star}$
	u_3	0.1974(1)	$0^{\dagger}$	-0.0083(2)	0.0074(3)	$0^{\dagger}$
OC2	u_1	0.5	$0^{\star}$	$0^{\star}$	$0^{\star}$	$0^{\dagger}$
	u_2	0.25	0.012(1)	$0^{\dagger}$	$0^{\dagger}$	0.023(2)
	u_3	0.1994(1)	$0^{\star}$	-0.0075(2)	0.0071(3)	$0^{\dagger}$
OS	u_1	0.2737(8)	$0^{\dagger}$	$0^{\star}$	$0^{\star}$	$0^{\dagger}$
	u_2	0.5	0.076(1)	$0^{\dagger}$	$0^{\dagger}$	0.020(2)
	u_3	0.1184(1)	$0^{\dagger}$	-0.0051(2)	0.0052(3)	$0^{\dagger}$
OB	u_1	0.145(3)	0.008(1)	-0.011(2)	-0.006(3)	0.005(3)
	u_2	0.103(4)	0.029(2)	0.062(2)	-0.037(3)	0.038(4)
	u_3	0.0575(6)	0.023(3)	-0.0050(3)	0.0058(3)	0.0011(6)
	P	0.522(7)	0.54(1)	-0.14(1)	$0^{\star}$	0.15(2)

TABLE VI. Refinement results for crystal *B*: positions (A_{ij},B_{ij}) and occupations (P). $0^{\star}$ were fixed during refinement because they were not significant. $0^{\dagger}$ were constrained by symmetry.

		$A_{2,0}(A'_{2,0})$	$B_{2,0}(B'_{2,0})$	$A_{1,1}(A'_{1,1})$	$B_{1,1}(B'_{1,1})$	$A_{1,-1}(A'_{1,-1})$	$B_{1,-1}(B'_{1,-1})$
Bi	u_1	$0^{\star}$	-0.0024(2)	0.0015(3)	0.0021(3)	$0^{\star}$	0.0035(3)
	u_2	0.0105(2)	-0.0248(5)	-0.0070(2)	-0.0177(2)	$0^{\star}$	0.0175(3)
	u_3	-0.0077(3)	$0^{\star}$	-0.00653(2)	$0^{\star}$	-0.00681(3)	$0^{\star}$
	P	-0.033(2)	$0^{\star}$	0.023(2)	-0.219(2)	0.057(2)	-0.207(2)
Sr	u_1	$0^{\dagger}$	$0^{\star}$	$0^{\star}$	$0^{\dagger}$	-0.0020(4)	$0^{\dagger}$
	u_2	0.0105(3)	$0^{\dagger}$	$0^{\dagger}$	0.0115(3)	$0^{\dagger}$	$0^{\star}$
	u_3	$0^{\dagger}$	$0^{\star}$	0.00079(4)	$0^{\dagger}$	$0^{\star}$	$0^{\dagger}$
Ca	u_1	$0^{\dagger}$	$0^{\dagger}$	$0^{\dagger}$	$0^{\dagger}$	$0^{\dagger}$	$0^{\dagger}$
	u_2	-0.0029(7)	$0^{\dagger}$	$0^{\dagger}$	$0^{\star}$	$0^{\dagger}$	-0.007(1)
	u_3	$0^{\dagger}$	$0^{\dagger}$	$0^{\dagger}$	$0^{\dagger}$	$0^{\dagger}$	$0^{\dagger}$
	P	$0^{\dagger}$	$0^{\dagger}$	0.021(6)	$0^{\dagger}$	-0.056(7)	$0^{\dagger}$
Cu	u_1	$0^{\dagger}$	$0^{\star}$	$0^{\dagger}$	$0^{\dagger}$	$0^{\star}$	$0^{\dagger}$
	u_2	$0^{\star}$	$0^{\dagger}$	$0^{\star}$	0.0012(5)	$0^{\dagger}$	-0.0058(6)
	u_3	$0^{\dagger}$	-0.00066(8)	0.00079(7)	$0^{\dagger}$	$0^{\star}$	$0^{\dagger}$
OS	u_1	$0^{\dagger}$	0.009(3)				
	u_2	0.034(2)	$0^{\dagger}$				
	u_3	$0^{\dagger}$	$0^{\star}$				

TABLE VII. Thermal displacement parameters for crystal *B* ($Å^2$).

	U_{iso}	U_{11}	U_{22}	U_{33}	U_{12}	U_{13}	U_{23}
Bi	0.0105(2)	0.0160(1)	0.0077(1)	0.0078(1)	0⋆	0⋆	0.0050(4)
Bi sin		0⋆	0.0133(2)	-0.0193(1)	0⋆	0⋆	0⋆
Bi cos		0.0064(1)	0.0242(2)	0⋆	0.0013(3)	-0.0022(1)	0⋆
Sr	0.0085(3)	0.0087(2)	0.0089(3)	0.0079(2)	0†	0.0024(2)	0†
Ca	0.0124(2)	0.0083(5)	0.0176(7)	0.0119(6)	0†	0⋆	0†
Cu	0.0123(1)	0.0015(3)	0.0087(4)	0.0047(4)	0†	-0.0006(3)	0†
OC1	0.0056(9)						
OC2	0.0089(9)						
OS	0.015(1)						
OB	0.021(1)						

assumed to exhibit an orthorhombic lattice. On the opposite side, the black triangles are systematically translated along **b**, involving a local monoclinic symmetry detected in the [001] pattern and the blurred contrast of the modulation in the [001] images (Fig. 5). This local variation of the stacking of undulated slabs can be interpreted as a residual disorder. It can be the origin of the poor agreement factor obtained for main reflections and for the presence in the diffraction pattern of diffuse scattering along **c** between satellite reflections.

The schematic representation of [BiO] layers projected along **c** (Fig. 7) shows the existence of double chains, parallel to the modulation direction, in the same way as in the pure bismuth cuprate or ferrite phases.[25] The usual description of the [BiO] layers as an alternation of ordered and disordered zones along the modulation direction **b** is slightly modified. The regions for *t* around 0 are characterized by a disorder resulting from the partial statistical occupation of two Bi and O split sites (Figs. 3 and 4). These regions are analogous to the disordered ones of the nonsubstituted compound. But around $t=0.5$, one observes a splitting of the two Bi and O sites. The slight splitting concerning the Bi atom was not seen previously in the undoped phases, but a corresponding disordered configuration for the oxygen atom was already described in the case of the ferrite phases.[25]

Between these two particular disordered regions, ordered configurations are observed with one Bi and one O site preferentially occupied. The corresponding Bi environment is characterized by two short and one intermediate Bi-O distances, in agreement with other Bi environments in different Bi oxide phases.[26] No evidence for an O site in a bridging position as in the lead-free phase could be found in the present refinement. In the rest of the structure, the OB site leaves its special position in the mirror plane orthogonal to **b** for a general position characterized by a harmonic occupation function so that the site is alternately occupied on each side of the mirror plane for $t<0.5$ and $t>0.5$, respectively (Fig. 4). This structural model was already proposed in the case of the ferrite phase.[25] It allows a modulation amplitude along *y* for the oxygen atom similar to the corresponding one for Bi. The difference between the regions with $t<0.5$ and $t>0.5$ lies in the relative position of the oxygen atom with respect to the Bi atom (either $y_O>y_{Bi}$ or $y_O<y_{Bi}$). These particular symmetrical configurations can be more clearly distinguished by calculating the position of an electronic lone pair of the Bi^{3+} ions according to electric-field estimations.[27] This position is very sensitive to the oxygen environment of the Bi^{3+} ion. For $0.2<t<0.4$ and $0.6<t<0.8$, this location is quite compatible with the known environments in related Bi oxides (Table VIII). One can see in Fig. 7 the alternate orientation of the lone pair along directions close to [110] and $[1\bar{1}0]$, respectively. The disordered configuration resulting from a statistical occupation of the split Bi and O sites near $t=0$ and 0.5 does not allow us to give a reliable estimation of the location of the lone pair in these regions.

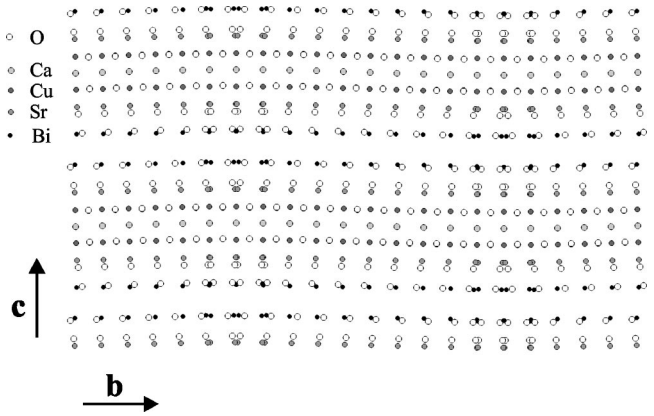

FIG. 2. Representation of the structure of crystal *A* projected along **a**.

According to this description, a schematic view of the [BiO] layers can be proposed (Fig. 8) where three types of regions can be distinguished: ordered ones with systematic orientation of the lone pairs along the *y* direction alternating in domains; and between these domains, two sorts of disordered zones (zone 1 and 3) resulting either the divergence (zone 1) or the convergence (zone 3) of the alternate orientation of the lone pairs. The quasiperiodic arrangement of the boundaries between these different zones is responsible for the incommensurate character of the structure. But one can easily imagine local variations in the relative length of the modulated zone 2, explaining the existence of disorder as evidenced from HREM observations or x-ray diffuse scattering, resulting in split sites in the structure refinement.

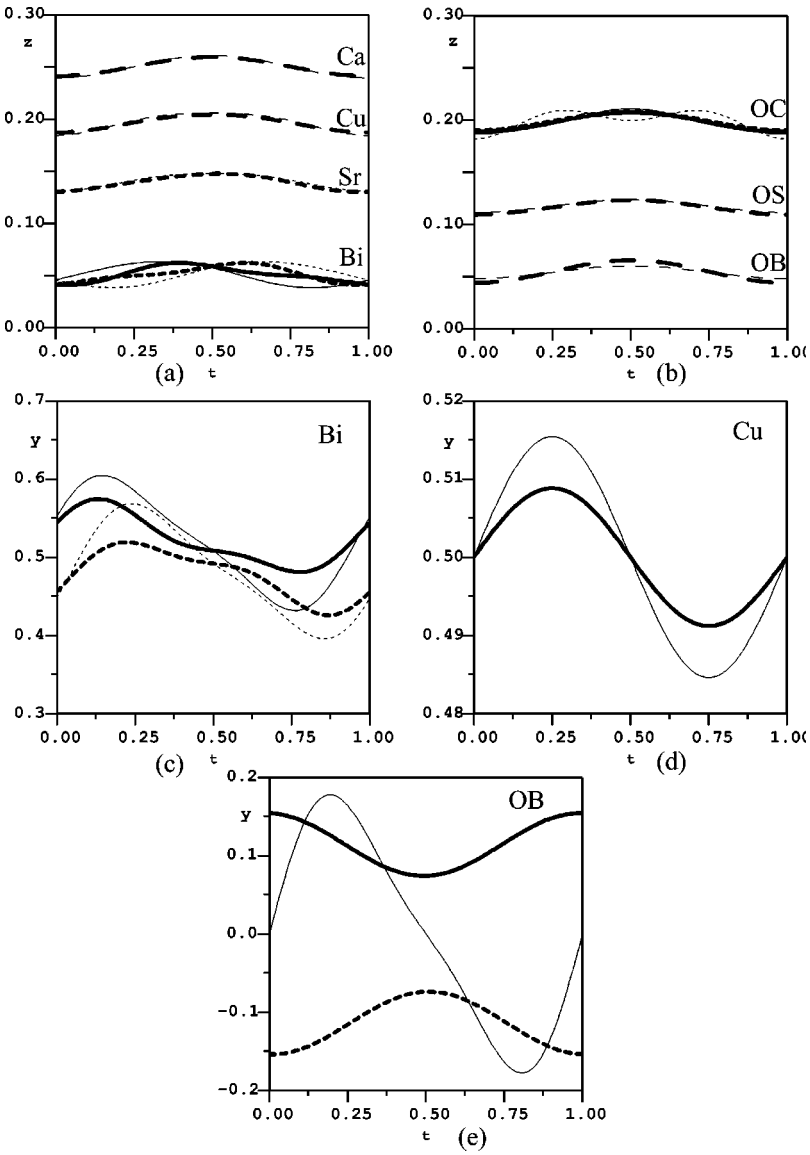

FIG. 3. Displacement modulation functions: (a) along *z* for cations, (b) along *z* for oxygen atoms, (c) along *y* for Bi, (d) along *y* for Cu, and (e) along *y* for oxygen atom OB in the [BiO] layers. Bold lines: Pb-type modulation (crystal *A*), and thin lines: undoped phase (Ref. 5).

Another difference with the pure bismuth phase concerns the copper environment. Interatomic Cu-O distances with the apical oxygen atom OS of the CuO_5 pyramids are in the present case quite constant between 2.43–2.49 Å. In the lead-free phase, this interval is larger (2.25–2.54 Å) and a shorter Cu-O apical distance was observed in the vicinity of the disordered BiO zone, which could be correlated with the insertion of an oxygen atom in the bridging position. Ca-O distances are also much more regular in the present case. The refined occupancy of the different atomic sites leads to the general formula $(Bi,Pb)_{2.09}Sr_2Ca_{0.89}Cu_{2.05}O_{7.97}$ in good agreement with the EDS analyses.

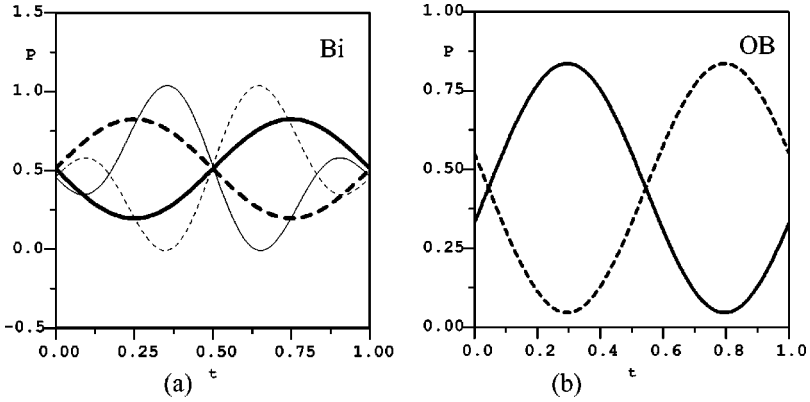

FIG. 4. Occupation modulation functions (a) for Bi and (b) for oxygen atom OB in the [BiO] layers. Bold lines: Pb-type modulation (crystal *A*), and thin lines: undoped phase (Ref. 5).

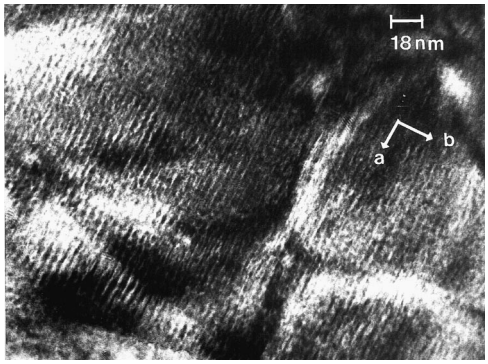

FIG. 5. [001] HREM image of crystal *A*.

B. The double-modulated structure of $Bi_{1.9}Pb_{0.4}Sr_{1.85}Ca_{0.8}Cu_2O_9$

We have shown that an intermediate Pb substitution rate between the lead-free modulated phase of type *I* and the monoincommensurate phase of type *II* leads to the existence of a new phase exhibiting a double modulation instead of a single modulation. Among the different types of satellite reflections, the well-sharpened satellites defined by $(\mathbf{q_I} \pm \mathbf{q_{II}})$ occupy the same positions as the diffuse-scattering intensities observed in the diffraction patterns of the corresponding undoped monoincommensurate phase. The value of the irrational part of the modulation vector (0.15) is intermediate between $\mathbf{q}_{\mathbf{I}irr}$ (0.21) and $\mathbf{q}_{\mathbf{II}irr}$ (0.11). One also observes a slight decrease in the $\mathbf{q}_{\mathbf{I}irr}$ value towards the rational 0.2 value. The presence of supplementary satellite reflections of type $(hkl \pm 1 \pm 1)$ cannot be fully explained from two types of domains exhibiting the first and second types of modulation, respectively. These reflections show that an actual double modulation is implied, at least in some parts of the crystal, requiring, then, a five-dimensional approach in the study of the modulated structure. In spite of the rational value 0.2 observed for $\mathbf{q_I}$, it is still preferable to consider this first commensurate superstructure as a modulated one, according to the first type of modulation. The effect of the double modulation on the structure can be explained from

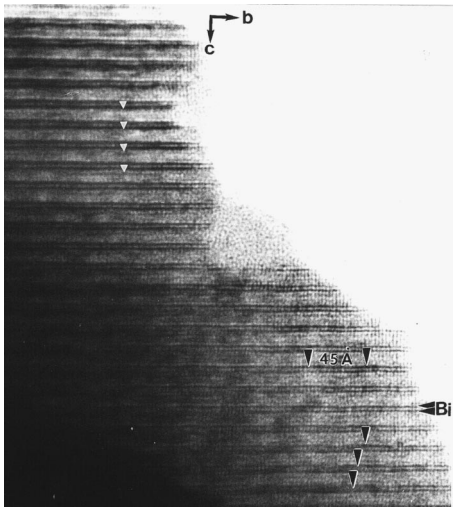

FIG. 6. [100] HREM image of crystal *A*.

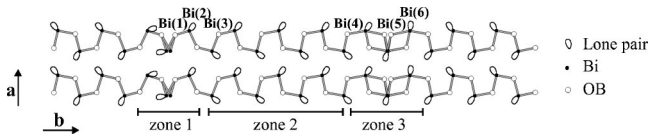

FIG. 7. Representation of [BiO] layers for crystal *A*. Only interatomic Bi-O distances less than 2.6 Å are drawn.

the separate action of the two modulations ($\overline{x_4}$ and $\overline{x_5}$ Fourier terms) and from a part of their interaction ($\overline{x_4} \pm \overline{x_5}$ Fourier terms). The previous accurate description of the two independent types of modulation allowed us to initiate proper displacement parameters and to obtain satisfactory final agreement factors within this double-modulation model.

The resulting structural features can be interpreted as a complex intermediate modulated state simultaneously involving two different internal centering conditions, two different modulation periods, and two types of displacements. Let us first describe the structural configuration of the [BiO] layers. They can still be described in the (**a**,**b**) plane by double chains parallel to **b** (Fig. 9), characteristic of the cuprate or ferrite phases. These chains still present an alternation of ordered and disordered regions, but in a more complex way. One can still define transition zones (TZ) periodically spaced along the **b** direction and characterized by partially occupied split sites and disorder phenomena. In some of these zones (called TZ1), oxygen atoms in bridging positions would be missing, in so far as no residual electron density could be found in Fourier difference maps. In fact, when looking at the different atomic sites and at their refined occupancy, these zones can be interpreted with an average description as locations where two different configurations are possible according to relative variable lengths of zones 1, 2, or 3.

A similar observation was outlined in the description of the type-*II* modulation. These transition zones correspond to a minimal distance between two adjacent [BiO] layers (interlayer Bi-Bi distances between 3.6–4.1 Å) as was the case in the type-*I* modulation. Other disordered zones (called TZ2), characterized by the simultaneous splitting of the Bi and OB sites, are similar to disordered zones of the type-*II* modulation.

TABLE VIII. Examples of Bi environments in ordered zones.

Bi(3)	OB(1)	OS	OB(2)	*E*(3)
OB(1)	**1.91**	3.14	3.07	2.39
OS	103.6	**2.08**	3.16	2.60
OB(2)	96.9	95.5	**2.18**	2.51
E(3)	121.3	125.3	107.2	**0.76**
Bi(4)	OB(3)	OS	OB(4)	E(4)
OB(3)	**2.10**	2.85	3.13	2.69
OS	84.8	**2.12**	3.04	2.87
OB(4)	91.2	88.2	**2.26**	2.87
E(4)	118.8	138.2	122.1	**0.93**

FIG. 8. Schematic representation of the orientation of the electronic lone pair in the [BiO] layers.

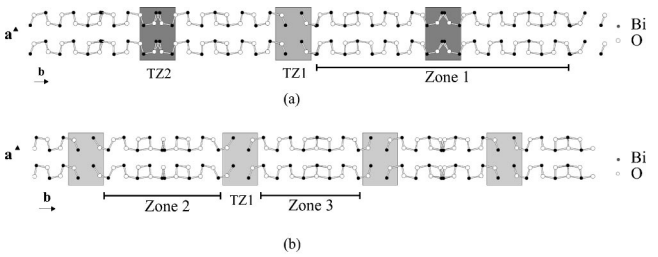

FIG. 9. Representation of [BiO] layers for crystal *B* in the (**a**,**b**) plane for (a) $z=0.05$ and (b) 0.22. Only Bi-O interatomic distances smaller than 2.6 Å are represented.

The projection of the double [BiO] layers along the **a** direction (Fig. 10) shows different possible configurations. In some areas, one [BiO] layer is rather flat while the adjacent one is characterized by a significant bending. In other areas, the relative undulations of two adjacent [BiO] layers are no more in phase than out of phase. The resulting stacking scheme looks like the configurations previously described either in the so-called ''collapsed'' ferrite phase[28] or in the monoclinic structure of the lead-free 2212 phase.[6] These configurations demonstrate the ability of these [BiO] layers to shift away from each other. The schematic drawing of the structure projected along **a** (Fig. 10) can be compared with electron microscopy observations.

Even if the double chain configuration is still observed at the level of the [SrO] layers, these last ones are much more regular, and disorder could not be observed concerning Sr and OS sites. Sr is eightfold or ninefold, coordinated with a regular calculated bond-valence sum close to 2.[29] Cu is always characterized by a pyramidal environment with four equatorial distances ranging from 1.84–1.99 Å and one apical distance varying from 2.20–2.54 Å. The situation concerning the [CuO] layers looks like the corresponding one in the pure 2212 phase. Minimal apical Cu-OS distances are still observed near transition disordered zones.

V. CONCLUSION

The structural study of a Pb-doped 2212 bismuth cuprate has been realized using x-ray-diffraction data with a single crystal characterized only by the Pb type modulation (absence of any rational component of the modulation vector; increased modulation period). The superspace symmetry has been defined, and modulated displacements and occupations have been refined. The results outline expected similarities with the corresponding modulated pure phase with analogous modulation amplitudes along *z*, but smaller ones along *y*. This discrepancy is explained by the corresponding increase in the modulation period and results in analogous waving of the BiO-SrO-CuO_2-Ca-CuO_2-SrO-BiO structural slabs. In the layer plane, the double chain configuration of the [BiO] and [SrO] layers is also observed.

The main difference directly results from the absence of any rational part for the modulation vector. As expected, this leads to an in-phase waving of the structural slabs instead of an out-of-phase one in the case of the lead-free phase. This new configuration allows more regular distances between two neighboring [BiO] layers. Nevertheless, shorter distances (2.1 Å) between slabs and longer ones (3.2 Å) within a BiO plane are not observed, as was previously predicted.[17] A second one is related to the increase in the modulation period. It involves the stabilization in the most important part of the crystal of a special configuration of the Bi atom. The disordered zones of the undoped phase with extra oxygen and shorter apical CuO distance are now replaced by two types of disordered zones that can be interpreted as a consequence of local variations in the modulation period and the length of the main modulated zones. This is also corroborated by HREM observations, which show irregularities in the modulated scheme of the layers.

The accurate knowledge of these two independent modulations allowed us to refine the structure of the double-

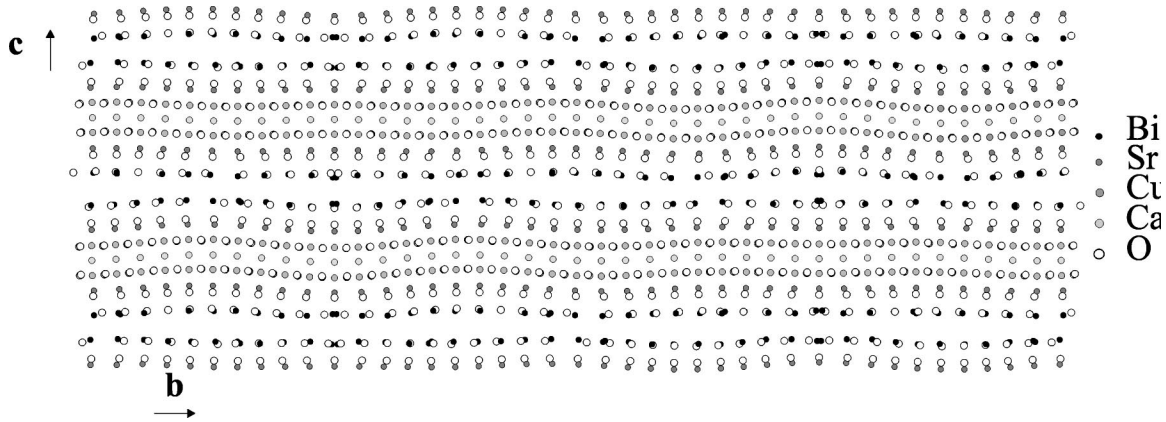

FIG. 10. Representation of the structure of crystal *B* projected along **a**.

modulated Pb-doped 2212 phase. It has been proven that according to the agreement obtained with the calculation of the intensity of the different types of satellite reflections, the corresponding structure is a proper double-modulated structure and cannot only be explained by the existence of two types of domains in the sample. In particular, different stacking schemes are possible between the slabs, with local apparent monoclinic symmetries, previously mentioned in different studies. Important disorder phenomena are still observed in this phase, in relation to the modulation and localized in specific zones. Still there, these disordered zones can be interpreted as varying boundaries between more regularly modulated regions. The existence and the description of this double-modulated phase gives a plausible explanation for the diffuse scattering frequently mentioned between main and satellite reflections of the lead-free phases. They are probably related to different stacking schemes of the structural slabs of the structure resulting, on a local scale and with a reduced correlation length, to an ''in-phase'' stacking of the corrugated layers.

[1] A. I. Beskrovnyi, M. Dlouha, M. Jirak, S. Vratislav, and E. Pollert, Physica C **171**, 79 (1990).

[2] A. Yamamoto, M. Onoda, E. Takayama-Muromachi, F. Izumi, T. Ishigaki, and H. Asano, Phys. Rev. B **42**, 4228 (1990).

[3] V. Petricek, Y. Gao, P. Lee, and P. Coppens, Phys. Rev. B **42**, 387 (1990).

[4] X. B. Kan and S. C. Moss, Acta Crystallogr., Sect. B: Struct. Sci. **48**, 122 (1992).

[5] D. Grebille, H. Leligny, A. Ruyter, Ph. Labbé, and B. Raveau, Acta Crystallogr., Sect. B: Struct. Sci. **B52**, 628 (1996).

[6] R. E. Gladyshevskii and R. Flukiger, Acta Crystallogr., Sect. B: Struct. Sci. **B52**, 38 (1996).

[7] W. B. Wu, L. B. Wang, J. S. Zhu, X. G. Li, G. E. Zhou, Y. T. Qian, Z. Y. Chen, and Y. H. Zhang, J. Appl. Phys. **76**, 2924 (1994).

[8] P. A. Miles, S. J. Kennedy, G. J. McIntyre, G. D. Gu, G. J. Russell, and N. Koshizuka, Physica C **280**, 66 (1997).

[9] S. T. Johnson, P. D. Hatton, A. J. S. Chowdury, B. M. Wanklyn, Y. F. Yan, Z. X. Zhao, and A. Marshall, Physica C **219**, 61 (1994).

[10] S. T. Johnson, P. D. Hatton, A. J. S. Chowdury, and B. M. Wanklyn, Solid State Commun. **94**, 261 (1995).

[11] J. Zhu, W. Wu, X. Sun, X. Zhao, G. Zhou, X. G. Li, and Y. Zhang, J. Phys.: Condens. Matter **8**, 1621 (1996).

[12] S. Ikeda, K. Aota, T. Hatano, and K. Ogawa, J. Appl. Phys. **27**, L2040 (1988).

[13] O. Eibl, Physica C **168**, 215 (1990).

[14] R. Ramesh, K. Remschnig, J. M. Tarascon, and S. M. Green, J. Mater. Res. **6**, 278 (1991).

[15] L. Pierre, J. Schneck, J. C. Tolédano, and C. Daguet, Phys. Rev. B **41**, 766 (1990).

[16] J. Schneck, J. C. Tolédano, L. Pierre, A. Litzler, D. Morin, J. Primot, H. Savary, and C. Daguet, J. Less-Common Met. **164-165**, 545 (1990).

[17] J.C. Tolédano, J. Schneck, and L. Pierre, *Geometry and Thermodynamics* (Plenum Press, New York, 1990), p. 335.

[18] H. Budin, O. Eibl, P. Pongratz, and P. Skalicky, Physica C **207**, 208 (1993).

[19] N. D. Zhigadlo, J. Phys.: Condens. Matter **6**, 1 (1994).

[20] Y. Hirotsu, Y. Ikeda, Y. Ichinose, S. Nagakura, T. Komatsu, and K. Matsushita, J. Electron Microsc. **40**, 147 (1991).

[21] P. Goodman, P. Miller, T. J. White, and R. L. Withers, Acta Crystallogr., Sect. B: Struct. Sci. **B48**, 376 (1992).

[22] Y. Gao, P. Lee, H. Graafsma, J. Yeh, P. Bush, V. Petricek, and P. Coppens, Chem. Mater. **2**, 323 (1990).

[23] T. Janssen, A. Janner, A. Looijjenga-Vos, and P. De Wolff, *1992 International Tables for Crystallography* (Kluwer, Dordrecht, 1992).

[24] V. Petricek, *1998 Crystallographic Computing System JANA98* (Academy of Sciences, Czech Republic, Prague, 1998).

[25] O. Pérez, H. Leligny, D. Grebille, J. M. Grenêche, Ph. Labbé, D. Groult, and B. Raveau, Phys. Rev. B **55**, 1236 (1997).

[26] N. Jakubowicz, O. Pérez, D. Grebille, and H. Leligny, J. Solid State Chem. **139**, 194 (1998).

[27] A. Verbaere, R. Marchand, and M. Tournoux, J. Solid State Chem. **23**, 383 (1978).

[28] O. Pérez, H. Leligny, D. Grebille, G. Baldinozzi, H. Graafsma, Ph. Labbé, and D. Groult, Phys. Rev. B **56**, 5662 (1997).

[29] N. E. Brese and M. O'Keefe, Acta Crystallogr., Sect. B: Struct. Sci. **47**, 192 (1991).